(article starts on next page)

Article

Volatility of a Ship's Emissions in the Baltic Sea Using Modelling and Measurements in Real-World Conditions

Oskari Kangasniemi [1,*], Pauli Simonen [1], Jana Moldanová [2], Hilkka Timonen [3], Luis M. F. Barreira [3], Heidi Hellén [3], Jukka-Pekka Jalkanen [3], Elisa Majamäki [3], Barbara D'Anna [4], Grazia Lanzafame [1,4], Brice Temime-Roussel [4], Johan Mellqvist [5], Jorma Keskinen [1] and Miikka Dal Maso [1]

[1] Aerosol Physics Laboratory, Physics Unit, Tampere University, 33720 Tampere, Finland; pauli.simonen@tuni.fi (P.S.); grazia.lanzafame@tuni.fi (G.L.); jorma.keskinen@tuni.fi (J.K.); miikka.dalmaso@tuni.fi (M.D.M.)
[2] IVL Swedish Environmental Research Institute, 41133 Gothenburg, Sweden; jana.moldanova@ivl.se
[3] Atmospheric Composition Research, Finnish Meteorological Institute, 00101 Helsinki, Finland; hilkka.timonen@fmi.fi (H.T.); luis.barreira@fmi.fi (L.M.F.B.); heidi.hellen@fmi.fi (H.H.); jukka-pekka.jalkanen@fmi.fi (J.-P.J.); elisa.majamaki@fmi.fi (E.M.)
[4] Aix Marseille University, CNRS, LCE, 13331 Marseille, France; barbara.danna@univ-amu.fr (B.D.); brice.temime-roussel@univ-amu.fr (B.T.-R.)
[5] Department of Earth, Space and Environment, Chalmers University of Technology, 41296 Gothenburg, Sweden; johan.mellqvist@chalmers.se
* Correspondence: oskari.kangasniemi@tuni.fi

Abstract: Shipping emissions are a major source of particulate matter in the atmosphere. The volatility of gaseous and particulate phase ship emissions are poorly known despite their potentially significant effect on the evolution of the emissions and their secondary organic aerosol (SOA) formation potential. An approach combining a genetic optimisation algorithm with volatility modelling was used on volatility measurement data to study the volatility distribution of a ship engine's emissions in real-world conditions. The fuels used were marine gas oil (MGO) and methanol. The engine was operated with 50% and 70% loads with and without active NOx after-treatment with selective catalytic reduction (SCR). The volatility distributions were extended to higher volatilities by combining the speciation information of the gas phase volatile organic compounds with particle phase volatility distributions and organic carbon measurements. These measurements also provided the emission factors of the gas and particle phase emissions. The results for the particle phase volatility matched well with the existing results placing most of the volatile organic mass in the intermediate volatile organic compounds (IVOC). The IVOCs also dominated the speciated gas phase. Partitioning of the emissions in the gas and particle phases was affected significantly by the total organic mass concentration, underlining the importance of the effect of the dilution on the phase of the emissions.

Keywords: marine emissions; atmospheric emissions; aerosols; volatility; volatility basis set

1. Introduction

Aerosols related to emissions from transport have a negative impact on both human health and the environment. Elevated levels of particulate matter have been shown to be connected to increased mortality (e.g., [1–4]) and to affect the radiation balance and thus climate change [5–7]. Marine traffic is a significant source of transport-related aerosols, and marine traffic emissions can contribute significantly to pollutant concentrations in the atmosphere, especially in coastal and harbour areas. Shipping contributes especially to sulphuric oxide (SOx), nitrogen oxide (NOx), and particulate matter emissions [8–10]. Gaining new information on ship emissions is especially important because the volume of marine traffic is increasing, although COVID-19 and the war in Ukraine are causing some uncertainties [11]. At the same time, the fuels used in the ship engines are being switched from heavy oil to cleaner alternatives, which affects the composition of the exhaust emission

aerosols [10,12]. In addition to the fuel, the engine load of a ship's engine changes the exhaust emission properties. Therefore, a ship's emissions near a harbour with a lower engine load may differ significantly from the emissions in the open sea with a higher engine load [10,13].

The current restrictions for NOx emissions, e.g., in Europe and North America, can be achieved only by using after-treatment devices. Selective catalytic reduction (SCR) is an effective technology to achieve this reduction. It is technology that uses a catalyst and ammonia, often in the form of urea, to reduce NOx to nitrogen and water. The use of such after-treatment methods has been shown to also have an effect on the emission of particles [14].

An exhaust aerosol released to the atmosphere evolves due to dilution and cooling, co-agulation, evaporation, deposition, and chemical processes. Understanding these processes is crucial to know the aerosol concentration and properties in an evolving exhaust plume, and to estimate the aerosol emission's effects on health and the environment. The volatility of species in fresh exhaust is one of the key factors determining how it will evolve. Fresh exhaust from a ship's engine contains organic compounds that have volatilities ranging from low (LVOCs) to very volatile (VOCs). Semi-volatile organic compounds (SVOCs) and intermediate volatile organic compounds (IVOCs) are of special interest since they can co-exist in both the gas and particle phases in the atmosphere. These compounds partition between the gas and particle phases depending on the total mass of each compound present and the effective saturation concentration values of these compounds at the prevailing temperature and pressure conditions along the plume [15,16]. For example, dilution will move organic matter from one phase to another. Shipping has been shown to be a major source of SVOCs and IVOCs [13,17,18]. Further, these organic compounds contribute to the formation of secondary organic aerosols (SOA). Unlike primary organic aerosols (POA), which are emitted to the atmosphere directly in the particle phase, SOA is formed from gas phase organic compounds via atmospheric oxidation and partitioning [15,19]. Since the atmospheric SOA formation mechanisms as well as the exact molecular compositions and evolution pathways of SVOCs and IVOCs are not fully understood, modelling efforts often underestimate the SOA formation in the atmosphere [20,21].

Fresh exhaust can contain thousands of different species. Trying to explicitly model or even experimentally characterise their chemistry in order to study the effects of volatility is challenging. Representing the volatilities of an emission as a volatility distribution rather than as individual values for specific compounds has been shown to be an effective approach [22–24]. The volatility basis set (VBS) approach groups species of similar volatilities together. Effective saturation concentration is used to characterise the volatility of these volatility bins.

Saturation vapour pressure-driven mass transfer between the gas and particle phases can be solved if the initial volatility distribution is known [25]. Obtaining this initial volatility distribution can be challenging. There is a lack of experimental data on aerosol volatilities. One approach to this problem is using existing emission inventories or experimentally identifying the species present in the emitted mixture and assigning volatility properties to these species. However, apart from the fact that identification of the VOC composition is associated with large uncertainties and incomplete mass closure, effective saturation concentration values are not available for the majority of organic compounds. Saturation concentrations are readily derived from the available saturation vapour pressure, but they describe a vapour over a pure liquid. Effective saturation concentration, however, applies to a vapour in a mixture and requires an activity coefficient [22,26,27]. Building a volatility distribution this way may therefore include some strong approximations. Another approach is to perform volatility measurements, for example with help of a thermodenuder, conditioning the measured aerosol at different temperatures, measuring the loss of the volatile PM, and comparing these results to an aerosol that has bypassed the thermodenuder. Simulation studies and optimisation methods can then be used to find the physical properties of an initial volatility distribution that match the measured

evaporation behaviour when used as an input in an evaporation model. In practice, this is typically challenging, since the evaporation of an aerosol depends on several properties such as the effective saturation concentration, the vaporisation enthalpy, and the mass accommodation coefficient. Several combinations of these can produce similar evaporation behaviour. One possible solution to this problem is using a genetic optimisation algorithm to find the volatility distribution and vaporisation enthalpies that match the measured behaviour as well as possible [28,29].

The VBS approach is readily used to model emissions of organic species and their effects on the atmosphere [23,30,31]. There are volatility distribution studies for on- and off-road engines [32–34] and laboratory experiments measuring the overall volatility of a ship's engine emissions [35,36]. However, ship exhaust volatility studies in real-world conditions are sparse. Huang et al. [17] measured the SVOC and IVOC volatility distributions aboard a large cargo vessel for high and low sulfur fuels and observed that a lower sulfur content corresponded to higher emissions of IVOC and SOA mass as well as higher volatility of the emissions.

This study offers novel information on ship exhaust emission volatilities in real-world conditions with different engine loads and fuels. In addition to providing volatility distributions for particle phase measurements, the species were identified in the gas phase to provide volatility distributions, including the more volatile species in the ship's emissions. The effect of the volatility on the partitioning of the emissions to the gas and particle phases was also studied to better understand a ship's engine emissions and their evolution in the atmosphere. This study adds to the rather sparse amount of information we have on the volatility of a ship's engine emissions, especially when operated in real-world conditions.

2. Methods

Ship exhaust emissions were measured aboard the Stena Germanica passenger/Ro-Pax ferry on September 2021, between Gothenburg, Sweden, and Kiel, Germany. Stena Germanica has four 4-stroke Sulzer 8ZAL40S diesel engines, which each provide 6000 kW for two controllable pitch propellers. The measurement setup used to study the volatility of the emissions with the thermodenuder is shown in Figure 1. The fuel used in most of the measurements was marine gas oil (MGO) with a low sulfur content of 0.095 wt %. Stena Germanica can also run on methanol, and emissions resulting from the use of this fuel were also measured. During the methanol operation, a small amount (6–14%) of MGO is used as a pilot fuel. Every emission was sampled after the selective catalytic reduction catalyst. The SCR was operated either with added urea (switched on) or without urea (switched off) to study the effect of the catalytic reduction. The investigated engine was operated to reach stable test periods with loads of about 25%, 50%, or 70%. The selection of the cases used in this paper is listed in Table 1.

To study the volatility of a particle phase emission from a ship's engine, the sample was first diluted using a porous tube diluter (PTD) and an ejector diluter. The sample was then led to a thermodenuder, which was heated to 250 °C [37]. The temperature was gradually brought down to 50 °C while simultaneously measuring the particle size distribution with two scanning mobility particle sizers (SMPS). The differential mobility analysers (DMA) and condensation particle counters (CPC) forming the SMPSs were DMA 3081 and CPC 3756 (TSI), for the long-SMPS, and DMA 3085 and CPC 3776 (TSI) for the nano-SMPS. The Soot-Particle Aerosol Mass Spectrometer (SP-AMS; Aerodyne Research Inc. [38], Billerica, MA, USA) measured the composition (total organic, sulphate, nitrate, ammonium, and chloride) and submicron particle mass concentration of the ship's emission, and the aethalometer (Model AE33; Magee Scientific, Berkeley, CA, USA) measured the equivalent black carbon (eBC) concentration. The evaporation of the aerosol could then be studied by comparing the measurement points downstream from the thermodenuder to an aerosol bypassing the thermodenuder. The mass fraction lost in the thermodenuder after calculation of the nominal thermodenuder losses is the fraction of the original aerosol evaporating at a given temperature. This, or conversely the mass fraction remaining in

the particle phase, can be used as the target data for the subsequent volatility modelling. The black carbon concentration measurements with the aethalometer were used to both estimate the losses inside the thermodenuder not caused by vaporisation, such as the wall losses, and to estimate the amount of black carbon in the sample.
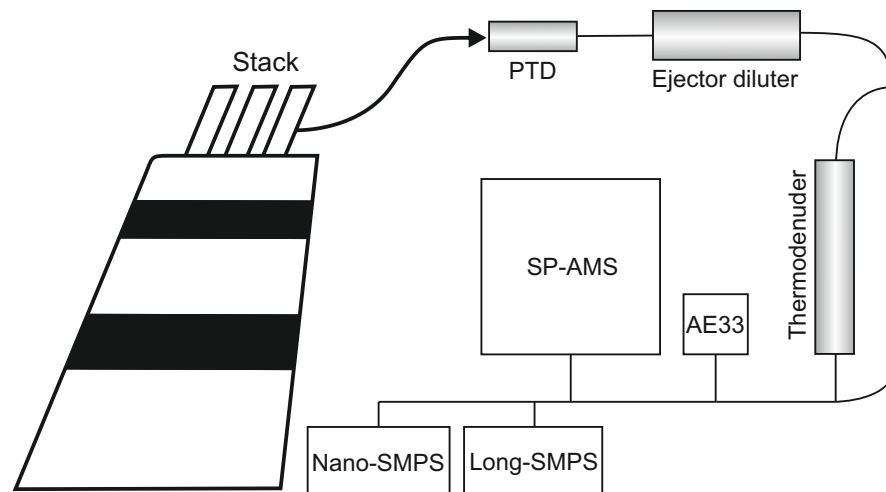
Figure 1. Setup used in the volatility measurements. The sample from the stack is diluted before it either enters or bypasses the thermodenuder. From there, the sample is led to an aethalometer, SP-AMS, and two SMPS setups.

Table 1. The different measurement cases used in the volatility experiments.

Fuel	Engine Load	After-Treatment
Marine gas oil	70%	SCR without urea
Marine gas oil	70%	SCR with urea
Marine gas oil	50%	SCR without urea
Marine gas oil	50%	SCR with urea
Methanol	50%	SCR without urea

Furthermore, offline sampling was also used to study the ship's exhaust. The organic carbon (OC) emissions for the MGO fuel were measured by collecting samples on quartz filters with a dilution ratio (DR) varying between 45 and 50. Because there was no filter collection for methanol post-catalyst, the OC emissions in this case were estimated using the SP-AMS. The filter samples were analysed using a thermal–optical carbon analyser (OCEC model 5 L; Sunset Laboratory). Five samples were taken for each measurement with the temperature of the diluted sample being 24–26 °C. To obtain the organic (particulate) matter (OM) concentration of the emission from the filter samples, the OC concentration was multiplied by 1.2 [39]. Gas characterisation was conducted using several different measurement techniques. Polyaromatic hydrocarbons (PAH) and dibenzothiophenes (DBT) were collected on polytetrafluoroethylene (PTFE) filters and XAD-2 adsorbent tubes for the gas phase. PAH and DBT samples were analysed at the Region Skåne laboratory with a gas chromatograph–mass spectrometer (GC-MS) comprised of an Agilent 5975C mass spectrometer and an Agilent 7890A gas chromatograph (Agilent Technologies). VOC and C_6-C_{10} alkane samples were collected using Tenax TA-Carbopack B sorbent tubes and C_2-C_6 non-methane hydrocarbons (NMHC) using evacuated stainless steel canisters. The canister and sorbent tube samples were analysed with gas chromatographs connected to a GC-MS and a flame ionisation detector (FID) at the Finnish Meteorological Institute. More detailed measurement descriptions are available [40].

The total hydrocarbon (THC) emissions in methane equivalents were measured using a flame ionisation detector (FID) on the raw (not diluted) exhaust that was led to the instrument using a heated line with a temperature of 180 °C, and the online VOC emissions

were measured with a proton transfer reaction time-of-flight mass spectrometer (PTR-ToF-MS 8000, Ionicon Analytics, Innsbruck, Austria). The sample exhaust was filtered for particulates before being diluted by a factor of 4 by an ejector diluter prior to the PTR-ToF-MS. The ejector, dilution air, and the sampling line were heated to at least 50 °C to minimise the wall losses of the gas phase species. Table S1 in the Supplementary Material contains all the identified species, their effective saturation concentrations, and the mass fractions for each of the five fuel, engine load, and after-treatment combinations. Not all the species were identified for each of the five measurement cases, which can also been seen in Table S1.

If an initial volatility distribution is known, the behaviour of an aerosol emission regarding evaporation can be simulated by solving the saturation vapour pressure-driven mass transfer between the gas and particle phase [25]. The mass flux of species i from the gas phase to the particle phase I_i is given by

$$I_i = \frac{2\pi d_p p M_i D_i \beta_i}{RT} ln\left(\frac{1 - \frac{p_{surf,i}}{p}}{1 - \frac{p_{far,i}}{p}}\right), \tag{1}$$

if $c_{p,i} > 0$, and $\frac{1 - \frac{p_{surf,i}}{p}}{1 - \frac{p_{far,i}}{p}} > 0$, or

$$I_i = \frac{2\pi d_p M_i D_i \beta_i}{RT} ln\left(p_{surf,i} - p_{far,i}\right), \tag{2}$$

if $c_{p,i} > 0$, and $\frac{1 - \frac{p_{surf,i}}{p}}{1 - \frac{p_{far,i}}{p}} \leq 0$.

Here, d_p is the particle diameter, p is the total gas pressure, M_i, D_i, and β_i are the molecular weight, diffusion coefficient, and correction factor for the transition regime for species i, respectively. R is the gas constant, and T is the temperature. $p_{surf,i}$ and $p_{far,i}$ are the partial pressures of species i at the particle surface and far away from the particle. $c_{p,i}$ is the mass concentration of species i in the particle phase.

To solve the initial volatility distribution from the evaporation data, we used a genetic optimisation algorithm [28,29]. We generated an initial population consisting of individuals with random volatility distributions. Population, here, refers to a set of volatility distributions. Each volatility distribution is an individual with randomly generated volatility bins. The mass fractions in the volatility bins of each individual add up to one. Each individual is used as input in an evaporation model to produce evaporation curves showing the fraction of mass that has not evaporated from the particle phase as a function of temperature. These curves are compared to a target function obtained from the evaporation seen in the thermodenuder measurements. Comparing the remaining mass after evaporation seen in the thermodenuder to the remaining mass according to the evaporation model and taking the mean square error gives each individual a fitness value. If desired, the algorithm can then keep on searching for new individuals even after reaching the wanted population size until it has found enough best fit candidates that have fitness values better than some best fit criterion.

After generating an initial population, the model chooses randomly, albeit with some bias towards the individuals with best fitness values, two parents or volatility distributions from the initial population to produce a child. The child inherits one half of its properties from each parent. In practise, this means that the child is a new volatility distribution made by taking half of the volatility bins from one parent distribution and half from the other (inheriting) and normalising this new distribution to one. It is also possible for the child to mutate, which means creating a completely new volatility distribution, as when creating the initial population. A child with a better fitness value than the worst existing individual in the population replaces that worst individual. If the fitness value of this individual child is worse than any of the individuals already in the population, the child is discarded. This

step is repeated over the whole population to produce a new generation. In this case, the word generation does not exactly match its normal definition, since older individuals fit enough to stay are also included in the next generation. The whole process is repeated over a chosen number of generations. The algorithm attempts to improve the fitness of the individuals, but the chance of mutation keeps the population varied to prevent the algorithm from converging to a local rather than global minimum. The general outline of the genetic algorithm is presented in Figure 2.
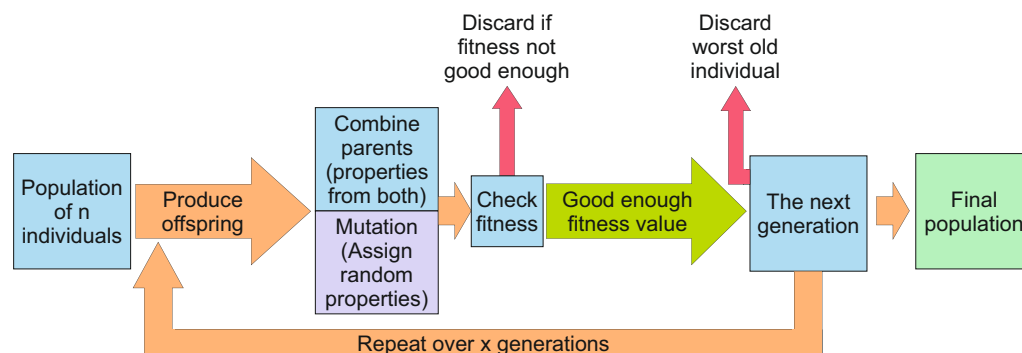
Figure 2. Flowchart describing the basic process of the genetic optimisation algorithm. An initial population of randomly generated individuals, i.e., volatility distributions, produces children taking one half of the volatility properties from each parent. The child can also mutate, which means drawing a completely new volatility distribution. These children are either accepted into the population or discarded based on how well their volatility behaviour matches a measured volatility when used as input in a volatility model. A new generation of individuals is created this way that, in turn, goes through the same process. The population of volatility distributions keeps on improving by discarding the worst individuals and replacing those with ones whose volatility behaviour better matches the measurement data. The aim of the process is to produce a volatility distribution that reproduces measurement data as accurately as possible when used in a volatility model.

To obtain a volatility distribution for a ship's exhaust emissions, measurements were carried out onboard the Stena Germanica ship. The volatility distribution we obtained from the thermodenuder experiments was the volatility distribution of a particle phase sample of the emission. The measured mass fractions remaining were loss-corrected based on the black carbon mass lost in the thermodenuder at different temperatures, since black carbon will not evaporate during the heat treatment. The SP-AMS and aethalometer data were used to calculate the fraction of particulate mass from the BC and organic compounds. The size distributions were measured using the two SMPS setups and scaling the total concentration according to the mass fractions as BC and organic compounds. These experimental data were then used as an input for the genetic optimisation algorithm.

Gas phase information is needed to obtain a full volatility distribution. Gas phase measurements were carried out to identify the gaseous species. All these species were then assigned effective saturation concentrations C_i^* values. Since there is a lack of knowledge when it comes to the exact effective saturation concentration values of most species, they were estimated based on their saturation vapour pressures and number of carbon and oxygen atoms [26]. The components were then divided into bins according to the effective saturation concentration values to obtain a volatility distribution as listed in Table S1.

To combine the two volatility distributions into one distribution, information on how these aerosols are divided between gas and particle phases is necessary. Organic aerosols with known volatility distribution and total concentration partitions to the gas and particle phases in equilibrium are calculated as in the following equation

$$\xi_i = \frac{1}{1 + \frac{C_i^*}{\sum C_{0,i}\xi_i}}, \tag{3}$$

where ξ_i is the partitioning coefficient of species i to the particle phase, and C_i^* and $C_{0,i}$ are the effective saturation concentration and the total mass concentration of species i, respectively. This equation can be solved iteratively for each species present in the aerosol but can also be used with the VBS approach, treating each volatility bin as an individual species.

Our approach was to solve partitioning based on the OM and THC measurements from the ship stack. The thermodenuder-derived volatility distribution was used together with the mass concentrations from the OM measurements to see how this aerosol partitioned to the gas and particle phases. The same was performed for the volatility distribution that was based on the identified species aboard the Stena Germanica, assuming that the total organic mass was the measured THC mass concentration. The particle and gas phase masses in each volatility bin from the OM and THC measurements were then compared. The volatility bins used for the OM and THC measurements were partly overlapping; therefore, there was a chance that some organic mass was double-counted. To account for this, the gas and particle phase concentrations for each bin were assumed to be the contributions from the OM and THC measurements with the higher organic mass concentration. The final volatility distribution was then formed by combining the chosen particle and gas phase concentrations for each bin and normalising the volatility distribution to the total organic mass obtained by summation of the individual bins. To test the feasibility of this approach, the particle phase mass fraction in the new VBS was compared to what it should be according to the partitioning equation. The process is illustrated in Figure 3. In all five cases, these two particle phase mass fractions compared reasonably well as can be seen in Figures S1–S5 in the Supplementary Materials.
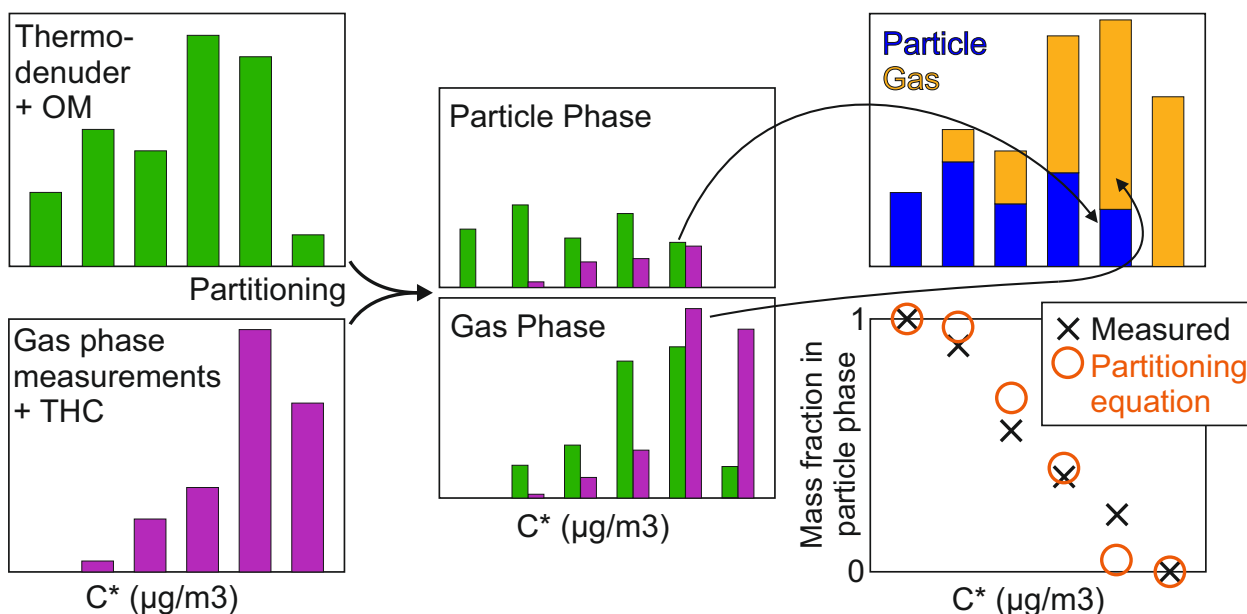

Figure 3. Schematic of the algorithm used to construct a full volatility distribution from the OM and THC measurements. Volatility distribution is created using the thermodenuder measurements with the OM concentration and the identified gas phase species together with the THC concentration. Partitioning to the gas and particle phases is then solved for all the bins and for each of the two distributions. For each bin, the particle and the gas phase concentration is chosen to be the larger contribution. The fraction of mass in the particle phase in this new volatility distribution is then compared to the fraction in the particle phase according to the partitioning equation using the same volatility distribution.

3. Results

*3.1. Volatility Distribution of a Ship's Emissions*

The genetic optimisation algorithm was used to find an initial distribution that would match the measured evaporation in the thermodenuder as well as possible when inserted into the evaporation model. The genetic optimisation algorithm was run 50 times for each case with a population size of 100 and over 25 generations. The final volatility distribution was the average of these 50 runs in each bin. The resulting evaporation curves together with the measurement points from the thermodenuder are shown in Figure 4. The measured remaining mass fractions were corrected based on the black carbon losses inside the thermodenuder, as described in the previous section.
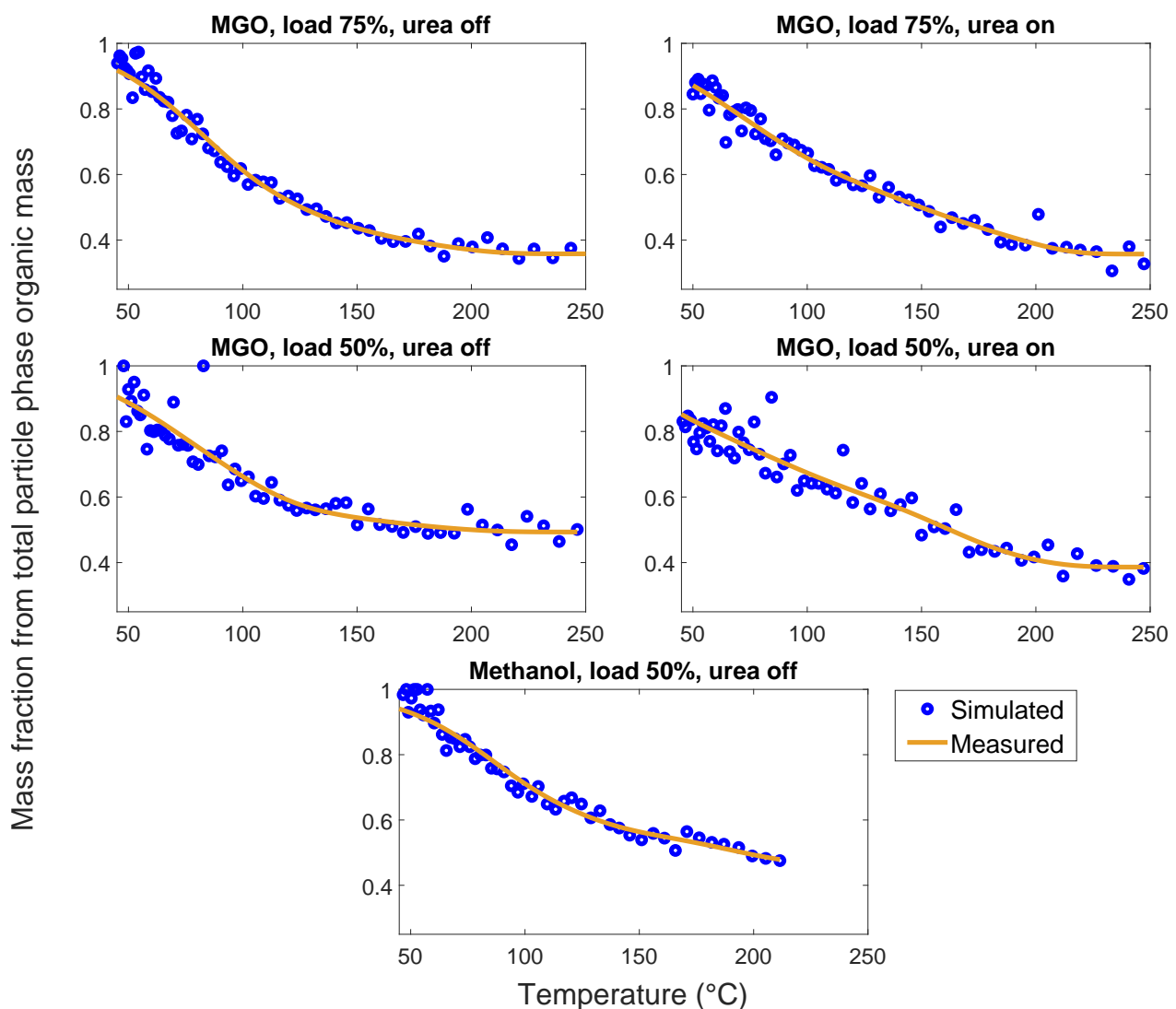
Figure 4. The evaporation curves obtained from the optimisation algorithm and the thermodenuder data compared to the measured data points from the thermodenuder measurements.

The volatility distributions obtained by using the genetic optimisation algorithm on the thermodenuder measurements are shown in Figure 5. The error bars are the standard deviations of the 50 genetic optimisation runs. In case of the MGO, the thermodenuder experiments were performed for 75% and 50% engine loads after SCR treatment either with or without urea injection. The nonvolatile fraction of the particle phase varied between 35 and 50%. Most of the volatile mass without urea injection was clearly in the IVOC volatility range, and the results followed a similar pattern with both engine loads and both types of fuels used. Urea treatment seemed to even out the volatility distribution with

the mass being divided more evenly between low-, semi-, and intermediate-volatile bins. When using a lower load, the nonvolatile fraction in the emission was slightly larger with and without urea. The volatility distribution of the particle phase emission when using methanol as a fuel with a 50% engine load was similar to the equivalent case using the MGO; although in the IVOC range, the most volatile bins had a smaller contribution to the distribution.
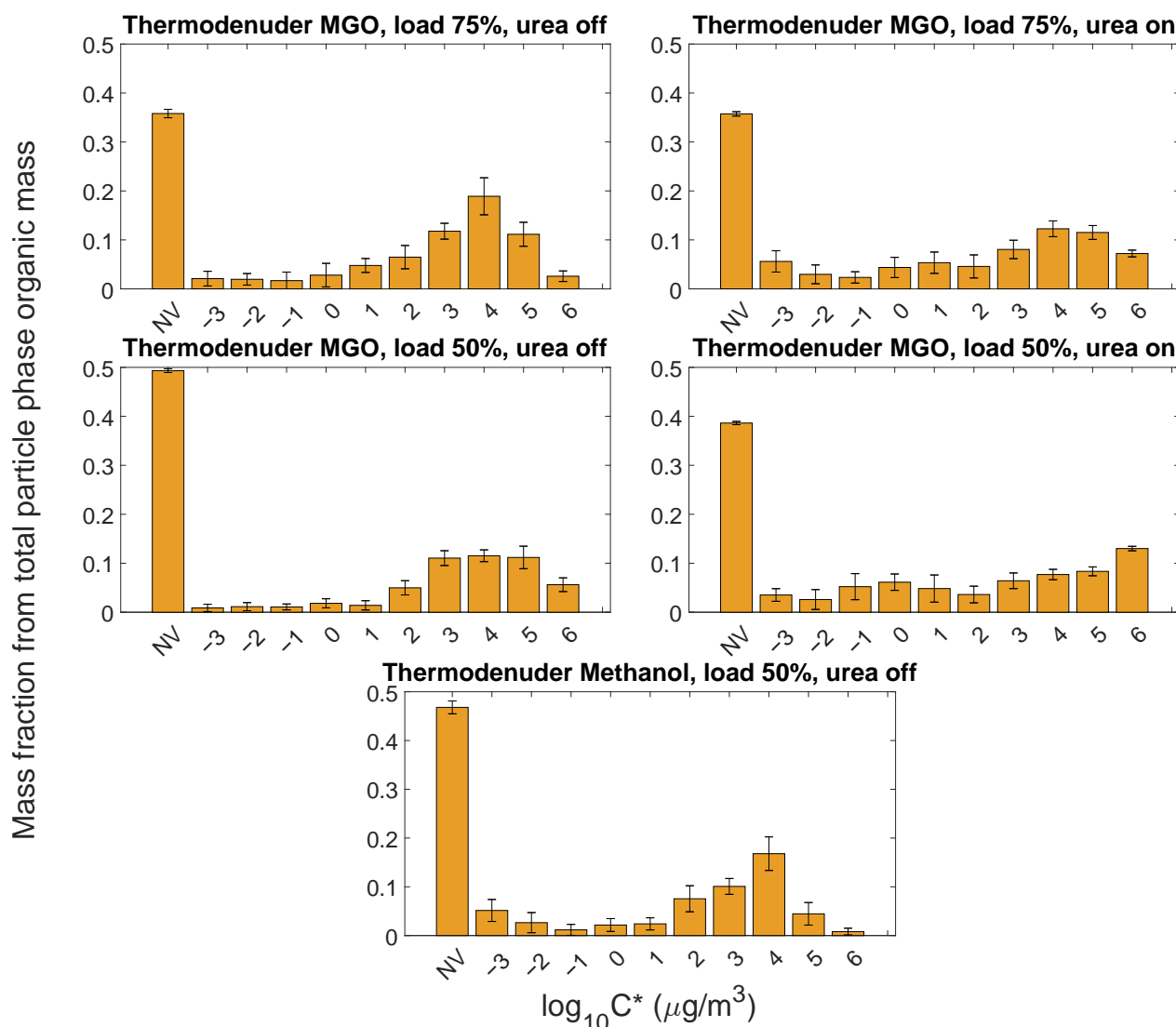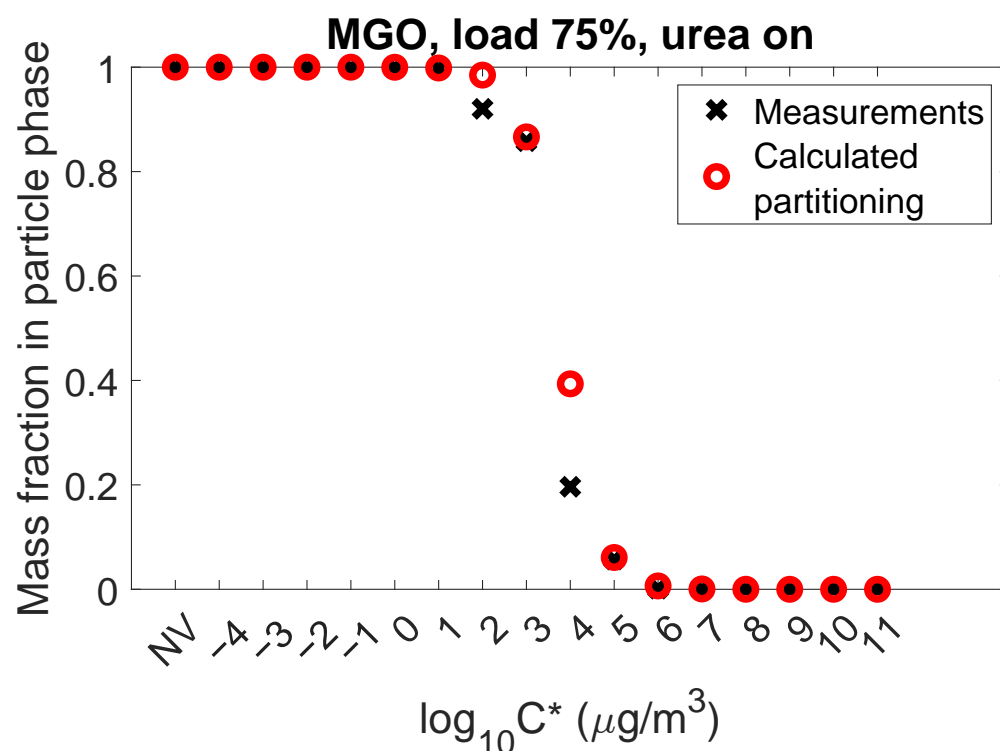

Figure 5. The volatility distributions of the particle phase samples used in the thermodenuder experiments shown as mass fractions from the total particle phase mass. The genetic optimisation algorithm was run 50 times for each case. The mass fraction from the particle phase organic mass is the average of these runs in each bin, and the error estimation comes from standard deviation of these runs.

The total volatility distribution based on both gas and particle phase measurements was constructed as described in the Methods section. The resulting volatility distributions are shown in Figure 6. In every case, a large amount of the mass was in bins 4 and 6. Based on the PTR-MS and GC-MS measurements, these high concentrations can be attributed to phthalic anhydride and maleic anhydride, respectively [40]. While the source of these anhydrides is not clear, phthalic anhydride could be an oxidation product from naphthalene [41]. Adding urea did not seem to have a large effect on the gaseous part of the distribution. When using methanol, there was a higher fraction of material in the very volatile bins.
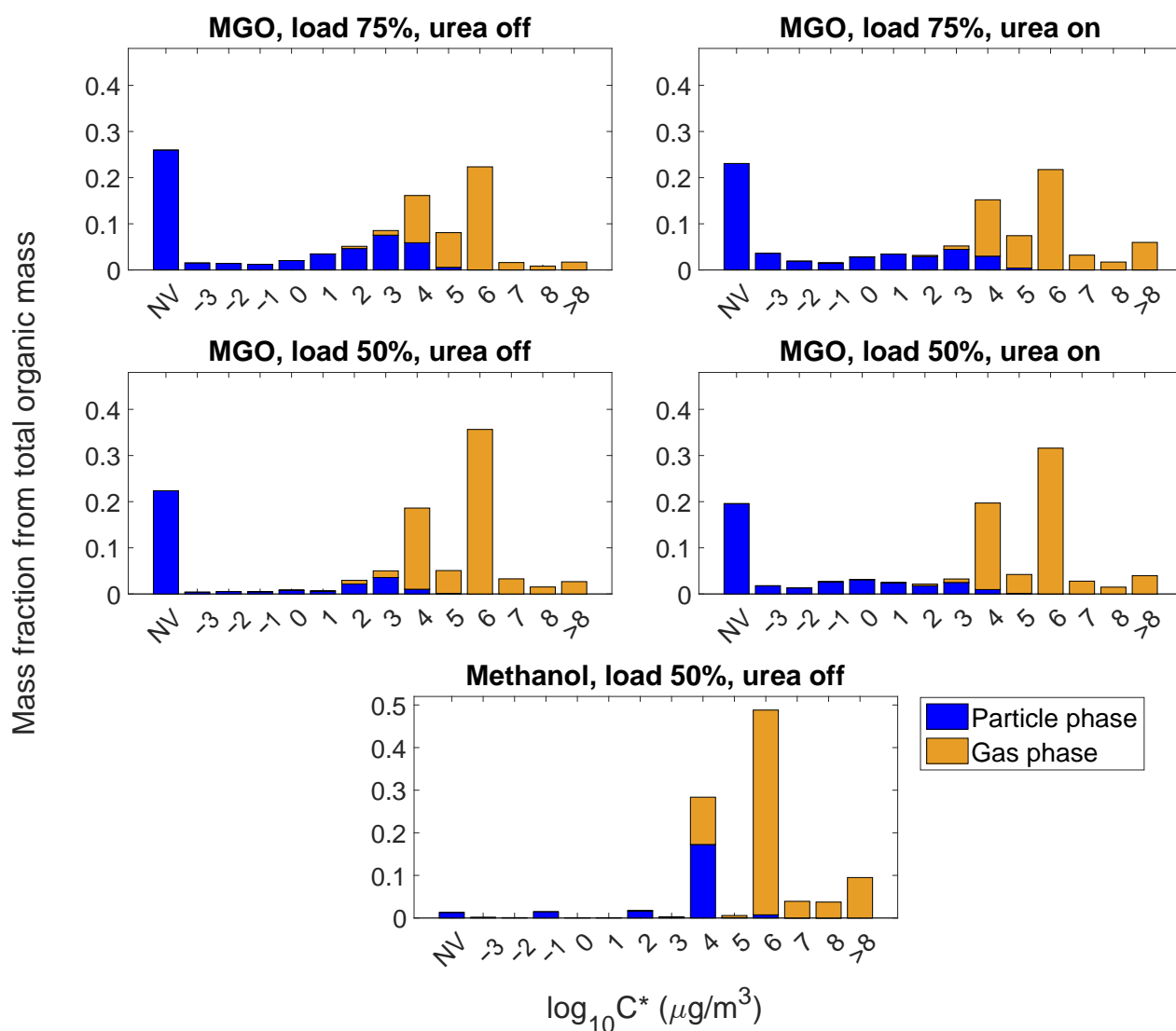
Figure 6. The combined volatility distributions as mass fractions from the total organic mass based on the OM and THC concentration measurements. The OM concentrations were applied to the VBS from the thermodenuder measurements and the THC to the VBS derived from gas phase measurements from the engine.

As an example, Figure 7 shows the partitioning to the particle phase for the MGO when using 75% engine load and the urea after-treatment. In this case, the results were similar, but the partitioning from the particle to the gas phase was very rapid when the volatility changed between bins 2 and 4. Similar plots can be seen for the rest of the measurement cases in Figures S1–S5 in the Supplementary Materials. It can be seen that although the curves followed similar trends, there was some discrepancy in the mentioned volatility bins. This could be explained by the uncertainty when it comes to the volatility fraction measurements but also by the volatility bin approach, which combines different volatilites and, as such, also creates uncertainty. The partitioning change between the intermediate volatility bins happens so rapidly that a large fraction of mass near the bin edge could cause some error, and in all the cases, in particular, bin 4 had a significant fraction of mass in it.

Figure 7. An example of the partitioning of a volatility distribution to the particle phase for an MGO with 75% engine load and urea treatment, constructed as described in the Methods section. The black crosses are the measured mass fractions in the particle phase based on the thermodenuder and the total hydrocarbon concentration measurements. These are compared to what the mass in the particle phase should be according to the partitioning equation.

Figure 6 shows the normalised volatility distributions and partitioning calculated for the sampling point directly after the emission when no dilution occurred. When the emission is released to the atmosphere, the partitioning evolves, since both the total mass concentration and the concentration of the constituent species will change due to dilution. The partitioning of the emissions with the previously derived volatility distributions to the particle phase as a function of the dilution is shown in Figure 8.

The emission factors, after calculating the partitioning in the gas and particle phases, are shown in Table 2. The table also shows the total mass concentration in the raw, i.e., undiluted exhaust. It should be noted that these are not the exact measured emission factors but the calculated values after partitioning based on the volatility distribution of the emission. For the MGO with 70% engine load, the addition of urea seemed to reduce the emission factor of the particle phase, while the gas phase emission factor was slightly higher. The total mass concentration was clearly lower when the engine load was 50%. The particle phase emission factor for the 50% engine load was also lower, and unlike with the 70% case, it was higher after urea treatment. The gas phase emission factor was similar to the 70% case and did not change significantly after the urea injection. For methanol, the total mass concentration was much higher than for the other cases. This was due to the much higher gas phase emission. In the undiluted case, some of the gas phase compounds partitioned to the particle phase.

The emission factors were also calculated using partitioning, corresponding to a diluted emission with a dilution ratio of 1000. As expected, the gas phase emission was increased, while the particle phase emission was reduced. In each case, the gas phase emission became the dominant one. For methanol, the particle phase emission factor was heavily reduced, since the volatility distribution consisted mostly of the more volatile bins.
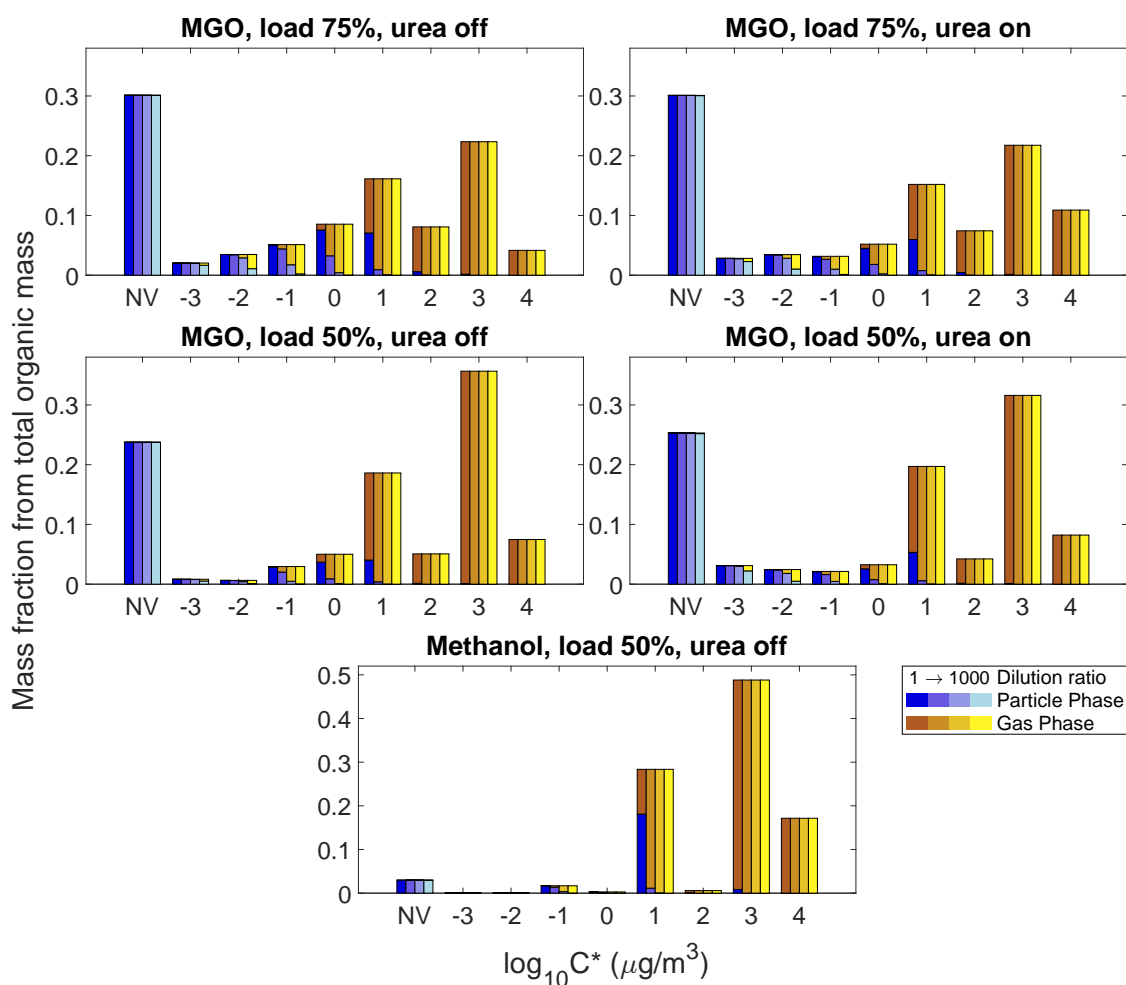
Partitioning for dilution ratio of 1-1000
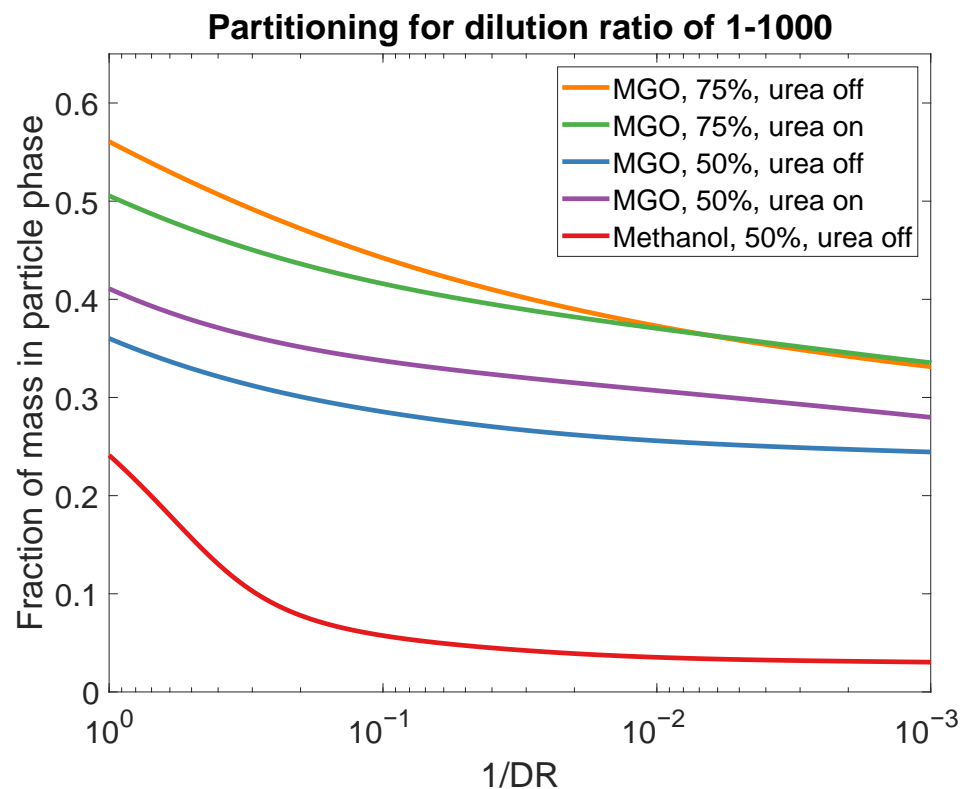
Figure 8. Partitioning of each of the measurement cases to the particle phase due to dilution. The total organic mass concentration of the emission is reduced with the dilution, which drives more mass from the particle to the gas phase.

Table 2. The total emissions as the mass concentration and emission factors for the particle and gas phases for the five measurement cases. The emission factors are shown as calculated at the point of release from the ship stack, assuming no dilution and assuming the partitioning of the emission is equivalent to it being diluted with DR = 1000.

	MGO, 70% Load, Urea Off	MGO, 70% Load, Urea On	MGO, 50% Load, Urea Off	MGO, 50% Load, Urea On	Methanol, 50% Load, Urea Off
Total concentration in the exhaust (mg/m^3)	13.9	12.8	7.7	9.0	73.2
Particle phase emission (mg/kg fuel)	208.4	174.7	77.0	101.3	248.1
Gas phase emission (mg CH$_4$eq./kg fuel)	284.7	327.1	276.2	268.2	1349.5
Particle phase emission (mg/kg fuel) (DR = 1000)	127.2	124.3	58.6	78.2	32.6
Gas phase emission (mg CH$_4$eq./kg fuel) (DR = 1000)	416.4	411.4	297.4	302.9	1700.9

The respective gas and particle phase fractions belonging to individual VBS bins also changed as the emissions diluted. Figure 9 shows the evolution of each measured volatility distribution for the dilution ratios of 1, 10, 100, and 1000. The particle phase was heavily reduced from the IVOC range already with the dilution ratio of 10 in each case. With higher dilution, practically all the particle mass was in the SVOC and lower volatility bins.

Figure 9. Bin-specific partitioning calculated for the five measurement cases with dilution ratios of 1, 10, 100, and 1000. The low-volatility bins, where all the mass is in the particle phase, have been combined as one bin. The most volatile bins have similarly been combined to one volatile bin.

3.2. Comparison to Existing Volatility Distributions

Huang et al. [17] measured the volatility distributions from ship engines in real-world conditions. They measured low-sulfur fuel emissions while leaving the port using a 50% engine load. While the fuels almost certainly were not the same, the MGO used in our study is also a type of low-sulfur fuel and can therefore be compared. The results from the two studies are presented in Table 3. When comparing the results from the thermodenuder measurements and the modelling, we readily observed that the results showed a somewhat higher mass fraction of nonvolatile mass. In the SVOC and IVOC ranges, both results were very similar with most of the volatile mass being in the IVOC range and peaking in the 4×10^4 μg/m^3 bin.

The Ship Traffic Emission Assessment Model (STEAM) is a model that can be used to evaluate the exhaust emissions of a marine vessel [42,43]. To estimate the chemical composition of the organic emission, STEAM distributes VOC species to four different groups whose relative contributions to the emission are based on measurements on marine as well as on off-road diesel engines [44–46]. While the VOC species STEAM uses are not exactly the same as the species identified aboard the Stena Germanica, a load-dependent VBS set was constructed for a STEAM VOC scheme in a similar manner as for the data obtained aboard the ship. In addition, the emission factors for load-dependent organic carbon and hydrocarbon emissions can be obtained from STEAM [47]. The total volatility distribution was built assuming all the organic carbon was nonvolatile material, while the hydrocarbon emission factor was divided into volatility bins according to the VBS built

for the STEAM VOC scheme. The figures for the 70% and 50% engine loads are shown in Figure 10.

Table 3. Mass fractions from the thermodenuder measurements and the modelling for the MGO using 50% load and without urea injection. The results are compared to a volatility distribution of a low sulfur fuel and a 50% engine load by Huang et al. [17].

$Log_{10}C^*$	MGO with 50% Engine Load, Urea Off	Huang et al. [17], Low Sulfur Fuel
Nonvolatile (<-1)	$51.3 \pm 0.7\%$	$36.2 \pm 1.9\%$
-1	$1.1 \pm 0.6\%$	$1.8 \pm 1.6\%$
0	$1.8 \pm 0.9\%$	$2.6 \pm 0.4\%$
1	$1.4 \pm 0.9\%$	$2.9 \pm 0.5\%$
2	$5.0 \pm 1.5\%$	$6.2 \pm 1.4\%$
3	$11.1 \pm 1.5\%$	$11.4 \pm 0.3\%$
4	$11.5 \pm 1.2\%$	$16.4 \pm 0.1\%$
5	$11.2 \pm 2.3\%$	$13.5 \pm 0.3\%$
6	$5.6 \pm 1.4\%$	$9.1 \pm 1.5\%$
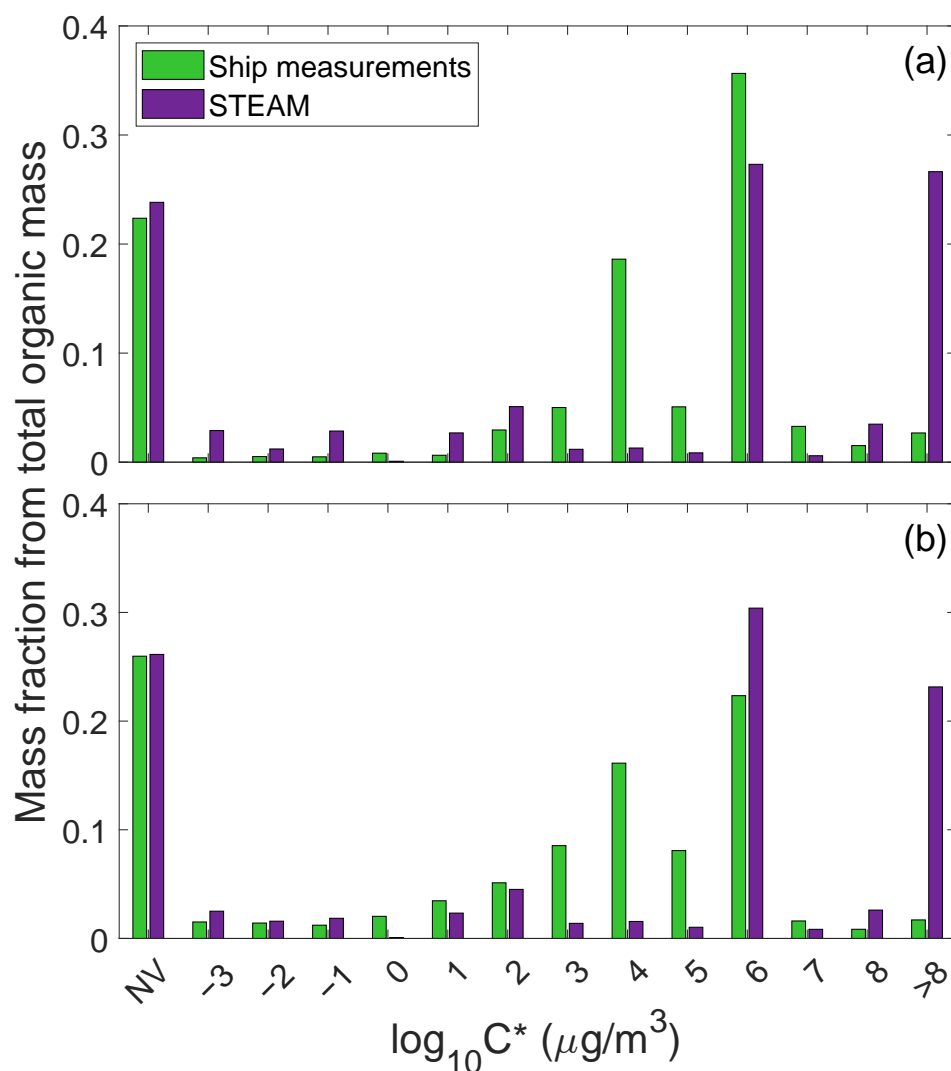
Figure 10. The volatility distribution from the ship's engine measurement compared to the volatility distribution from the STEAM model for the (**a**) 50% engine load and the (**b**) 70% engine load.

The amount of nonvolatile material was similar in both cases. With a 50% engine load, the STEAM predicted somewhat higher amounts of low- and semi-volatile material, while with a 70% engine load, the differences were small. Notable differences can be seen in the IVOC range (300–3 × 10^6 μg/m^3), where the mass fractions were clearly higher for the volatility distributions based on ship measurements using both engine loads, with bin 6 being an exception. In particular, bin 4 showed much higher mass fractions. An explanation for this could be that the sample measured aboard Stena Germanica was already somewhat oxidised due to the presence of the SCR. As mentioned, the high mass concentrations in bin 4 from the ship measurements was due to phthalic anhydride. Since phthalic anhydride is an oxidation product of naphthalene, this could explain the large difference in this bin size. In the STEAM distribution, the high fraction of bin 6 was due to naphtalene. This was present in much lesser quantities in the ship's engine measurements, where most of the mass in bin 6 was due to maleic anhydrade. The maleic anhydride's relative contribution seemed to be larger, when the engine load was lower. The absence of maleic hydride from the STEAM would explain why bin 6 had more mass then the STEAM predicted with a lower engine load and less with a higher engine load. The high amount of very volatile material in the STEAM distribution can be attributed to formaldehyde. This is probably because the VOC distribution from Agrawal et al. (2008) [44] is used in the STEAM to describe the VOC speciation. The ship used was a Suezmax crude oil tanker using a 15.8 MW two-stroke main engine and 2.85% S Heavy Fuel Oil [44]. This tanker also had smaller four-stroke auxiliary engines, which used MGO as fuel. The emission measurements for both the main and auxiliary engines were reported in their work, and the VOC speciation of the main engine was implemented in the STEAM. It should be noted that the main engine measurements of Agrawal et al. indicated high emissions of formaldehyde, whereas the measurements for the auxiliary engine running on MGO indicated much lower formaldehyde emissions and were more similar to the results of the current work. The differences in the VOC emission profiles of the main and auxiliary engines [44] indicated that there may be a need to differentiate between VOC volatility profiles of the residual and distillate fuels and to conduct more measurements to understand the difference between VOC emission profiles of two-stroke and four-stroke engines running on the same fuel.

4. Discussion

The volatility distributions from using the genetic optimisation algorithm and the evaporation model on volatility experiments conducted with a thermodenuder were very similar to those measured by Huang et al. [17] for low sulfur fuels with a sulfur content of 0.38 wt %. It should be noted that they used a very different method in their analysis. Their volatility distribution was obtained by using gas chromatography retention times on samples collected on thermal desorption tubes, while the volatility distributions used in this work were based on the evaporation of an aerosol sample in a thermodenuder. The fact that the results from these two different approaches were so similar is encouraging, and further studies comparing different approaches using the same samples would be useful to confirm these results.

The results for a larger engine load followed a similar pattern to the results for methanol as fuel further indicating that combining measured volatility data with a modelling approach is a feasible way to study the volatility of a particle phase emission.

The low-sulfur fuels all produced volatility distributions with a significant amount of volatility being in the IVOC range. This would suggest there is a high relative potential for SOA formation. Dilution quickly causes the IVOC species to partition to the gas phase, but the treatment here did not consider the atmospheric reactions that these species may undergo. It is likely that the larger IVOC molecules react in the atmosphere faster than other VOCs. Atmospheric oxidation can produce lower volatility material, and aging studies would be necessary to better understand the effect of chemical reactions on the volatility and partitioning of an emission.

The emission factors for the organic gas and particle phase emissions can be very different depending on the dilution conditions. This should be taken into account when trying to understand the particle and gas phase emissions from transport and their impact on the air quality of the surrounding areas. The effect of partitioning should be considered both when designing the measurements and interpreting the results and their impacts on particular in emission inventories, where lack of consistency in the interpretation of the phase state of the emissions may lead to double-counting of the emissions of organic matter. To properly understand how the volatility of an emission changes after it is released in the atmosphere, both the effect of the dilution and the atmospheric chemistry need to be taken into account.

Supplementary Materials: The following supporting information can be downloaded at: https://www.mdpi.com/article/10.3390/atmos14071175/s1, Figure S1: Combining the volatility distribution for the MGO 75% engine load without the urea after-treatment; Figure S2: Combining the volatility distribution for the MGO 75% engine load with the urea after-treatment; Figure S3: Combining the volatility distribution for the MGO 50% engine load without the urea after-treatment; Figure S4: Combining the volatility distribution for the MGO 50% engine load with the urea after-treatment; Figure S5: Combining the volatility distribution for the methanol 75% engine load without the urea after-treatment; Table S1: Identified gas phase organic species, their effective saturation concentrations, volatility bins, and mass fractions

Institutional Review Board Statement: Not applicable.

Informed Consent Statement: Not applicable.

Data Availability Statement: The data presented are available on request from the corresponding author.

Conflicts of Interest: The authors declare no conflict of interest. The funders had no role in the design of the study; in the collection, analyses, or interpretation of data; in the writing of the manuscript; or in the decision to publish the results.

Abbreviations

The following abbreviations are used in this manuscript:

BC	Black Carbon
CPC	Condensation Particle Counter
DMA	Differential Mobility Analyser
DBT	Dibenzothiophenes
eBC	Equivalent Black Carbon
FID	Flame Ionisation Detector

GC-MS	Gas Chromatography Mass Spectrometer
IVOC	Intermediate Volatile Organic Compound
LVOC	Low Volatile Organic Compound
MGO	Marine Gas Oil
NMHC	Non-Methane Hydrocarbon
OC	Organic Carbon
OM	Organic (Particulate) Matter
PAH	Polyaromatic Hydrocarbon
POA	Primary Organic Aerosol
PTD	Porous Tube Diluter
PTFE	Polytetrafluoroethylene
PTR-ToF-MS	Proton Transfer Reaction—Time of Flight—Mass Spectrometer
SCR	Selective Catalytic Reduction
SMPS	Scanning Mobility Particle Sizer
SOA	Secondary Organic Aerosol
SP-AMS	Soot Particle Aerosol Mass Spectrometer
STEAM	Ship Traffic Emission Assessment Model
SVOC	Semi-Volatile Organic Compound
THC	Total Hydrocarbons
VBS	Volatility Basis Set
VOC	Volatile Organic Compound

References

1. Pope, C.A.; Dockery, D.W. Health Effects of Fine Particulate Air Pollution: Lines that Connect. *J. Air Waste Manag. Assoc.* **2006**, *56*, 709–742. [CrossRef] [PubMed]
2. Caiazzo, F.; Ashok, A.; Waitz, I.A.; Yim, S.H.L.; Barrett, S.R.H. Air pollution and early deaths in the United States. Part I: Quantifying the impact of major sectors in 2005. *Atmos. Environ.* **2013**, *79*, 198–208. [CrossRef]
3. Pieters, N.; Koppen, G.; Van Poppel, M.; De Prins, S.; Cox, B.; Dons, E.; Nelen, V.; Panis, L.I.; Plusquin, M.; Schoeters, G.; et al. Blood Pressure and Same-Day Exposure to Air Pollution at School: Associations with Nano-Sized to Coarse PM in Children. *Environ. Health Perspect.* **2015**, *123*, 737–742. [CrossRef] [PubMed]
4. Lelieveld, J. Clean Air in the Anthropocene. *Faraday Discuss.* **2017**, *200*, 693–703. [CrossRef] [PubMed]
5. Ramanathan, V.; Feng, Y. Air pollution, greenhouse gases and climate change: Global and regional perspectives. *Atmos. Environ.* **2009**, *43*, 37–50. [CrossRef]
6. Seinfeld, J.H.; Bretherton, C.; Carslaw, K.S.; Coe, H.; DeMott, P.J.; Dunlea, E.J.; Feingold, G.; Ghan, S.; Guenther, A.B.; Kahn, R.; et al. Improving Our Fundamental Understanding of the Role of Aerosol-cloud Interactions in the Climate System. *Proc. Natl. Acad. Sci. USA* **2016**, *113*, 5781–5790. [CrossRef]
7. Bellouin, N.; Quaas, J.; Gryspeerdt, E.; Kinne, S.; Stier, P.; Watson-Parris, D.; Boucher, O.; Carslaw, K.S.; Christensen, M.; Daniau, A.-L.; et al. Bounding Global Aerosol Radiative Forcing of Climate Change. *Rev. Geophys.* **2016**, *58*, e2019RG000660. [CrossRef]
8. Sofiev, M.; Winebrake, J.J.; Johansson, L.; Carr, E.W.; Prank, M.; Soares, J.; Vira, J.; Kouznetsov, R.; Jalkanen, J.-P.; Corbett, J.J. Cleaner fuels for ships provide public health benefits with climate tradeoffs. *Nat. Commun.* **2018**, *9*, 406. [CrossRef]
9. Becagli, S.; Anello, F.; Bommarito, C.; Cassola, F.; Calzolai, G.; Di Iorio, T.; di Sarra, A.; Gómez-Amo, J.-L.; Lucarelli, F.; Marconi, M.; et al. Constraining the ship contribution to the aerosol of the central Mediterranean. *Atmos. Chem. Phys.* **2017**, *17*, 2067–2084. [CrossRef]
10. Moldanová, J.; Fridell, E.; Winnes, H.; Holmin-Fridell, S.; Boman, J.; Jedynska, A.; Tishkova, V.; Demirdjian, B.; Joulie, S.; Bladt, H.; et al. Physical and chemical characterisation of PM emissions from two ships operating in European Emission Control Areas. *Atmos. Meas. Tech.* **2013**, *6*, 3577–3596. [CrossRef]
11. Review of Maritime Transport 2022. United Nations Conference on Trade and Development. Available online: https://unctad.org/webflyer/reviewmaritime-transport-2021 (accessed on 5 April 2023).
12. Streibel, T.; Schnelle-Kreis, J.; Czech, H.; Harndorf, H.; Jakobi, G.; Jokiniemi, J.; Karg, E.; Lintelmann, J.; Matuschek, G.; Michalke, B.; et al. Aerosol emissions of a ship diesel engine operated with diesel fuel or heavy fuel oil. *Environ. Sci. Pollut. Res.* **2017**, *24*, 10976–10991. [CrossRef]
13. Liu, Z.; Chen, Y.; Zhang, Y.; Zhang, F.; Feng, Y.; Zheng, M.; Li, Q.; Chen, J. Emission Characteristics and Formation Pathways of Intermediate Volatile Organic Compounds from Ocean-Going Vessels: Comparison of Engine Conditions and Fuel Types. *Environ. Sci. Technol.* **2022**, *56*, 12917–12925. [CrossRef]
14. Lehtoranta, K.; Vesala, H.; Koponen, P.; Korhonen, S. Selective Catalytic Reduction Operation with Heavy Fuel Oil: NOx, NH3, and Particle Emissions. *Environ. Sci. Technol.* **2015**, *49*, 4735–4741. [CrossRef]

15. Robinson, A.L.; Donahue, N.M.; Shrivastava, M.K.; Weitkamp, E.A.; Sage, A.M.; Grieshop, A.P.; Lane, T.E.; Pierce, J.R.; Pandis, S.N. Rethinking Organic Aerosols: Semivolatile Emissions and Photochemical Aging. *Science* **2007**, *315*, 1259–1262. [CrossRef] [PubMed]

16. Saha, P.K.; Khlystov, A.; Grieshop, A.P. Downwind evolution of the volatility and mixing state of near-road aerosols near a US interstate highway. *Atmos. Chem. Phys.* **2018**, *18*, 2139–2154. [CrossRef]

17. Huang, C.; Hu, Q.; Li, Y.; Tian, J.; Ma, Y.; Zhao, Y.; Feng, J.; An, J.; Qiao, L.; Wang, H.; et al. Intermediate Volatility Organic Compound Emissions from a Large Cargo Vessel Operated under Real-World Conditions. *Environ. Sci. Technol.* **2018**, *52*, 12934–12942. [CrossRef]

18. Wu, L.; Ling, Z.; Liu, H.; Shao, M.; Lu, S.; Wu, L.; Wang, X. A Gridded Emission Inventory of Semi-Volatile and Intermediate Volatility Organic Compounds in China. *Sci. Total Environ.* **2021**, *761*, 106546. [CrossRef]

19. Zhao, Y.; Hennigan, C.J.; May, A.A.; Tkacik, D.S.; de Gouw, J.A.; Gilman, J.B.; Kuster, W.C.; Borbon, A.; Robinson, A.L. Intermediate-Volatility Organic Compounds: A Large Source of Secondary Organic Aerosol. *Environ. Sci. Technol.* **2014**, *48*, 13743–13750. [CrossRef] [PubMed]

20. Ortega, A.M.; Hayes, P.L.; Peng, Z.; Palm, B.B.; Hu, W.; Day, D.A.; Li, R.; Cubison, M.J.; Brune, W.H.; Graus, M.; et al. Real-Time Measurements of Secondary Organic Aerosol Formation and Aging from Ambient Air in an Oxidation Flow Reactor in the Los Angeles Area. *Atmos. Chem. Phys.* **2016**, *16*, 7411–7433. [CrossRef]

21. Ling, Z.; Wu, L.; Wang, Y.; Shao, M.; Wang, X.; Huang, W. Roles of Semivolatile and Intermediate-Volatility Organic Compounds in Secondary Organic Aerosol Formation and Its Implication: A Review. *J. Environ. Sci.* **2022**, *114*, 259–285. [CrossRef]

22. Donahue, N.M.; Robinson, A.L.; Stanier, C.O.; Pandis, S.N. Coupled Partitioning, Dilution, and Chemical Aging of Semivolatile Organics. *Environ. Sci. Technol.* **2006**, *40*, 2635–2643. [CrossRef]

23. Han, Z.; Xie, Z.; Wang, G.; Zhang, R.; Tao, J. Modeling Organic Aerosols over East China Using a Volatility Basis-Set Approach with Aging Mechanism in a Regional Air Quality Model. *Atmos. Environ.* **2016**, *124*, 186–198. [CrossRef]

24. Ciarelli, G.; Aksoyoglu, S.; Crippa, M.; Jimenez, J.-L.; Nemitz, E.; Sellegri, K.; Äijälä, M.; Carbone, S.; Mohr, C.; O'Dowd, C.; et al. Evaluation of European Air Quality Modelled by CAMx Including the Volatility Basis Set Scheme. *Atmos. Chem. Phys.* **2016**, *16*, 10313–10332. [CrossRef]

25. Riipinen, I.; Pierce, J.R.; Donahue, N.M.; Pandis, S.N. Equilibration time scales of organic aerosol inside thermodenuders: Evaporation kinetics versus thermodynamics. *Atmos. Environ.* **2010**, *44*, 597–607. [CrossRef]

26. Donahue, N.M.; Epstein, S.A.; Pandis, S.N.; Robinson, A.L. A Two-Dimensional Volatility Basis Set: 1. Organic-Aerosol Mixing Thermodynamics. *Atmos. Chem. Phys.* **2011**, *11*, 3303–3318. [CrossRef]

27. Epstein, S.A.; Riipinen, I.; Donahue, N.M. A Semiempirical Correlation between Enthalpy of Vaporization and Saturation Concentration for Organic Aerosol. *Environ. Sci. Technol.* **2010**, *44*, 743–748. [CrossRef] [PubMed]

28. Tikkanen, O.-P.; Hämäläinen, V.; Rovelli, G.; Lipponen, A.; Shiraiwa, M.; Reid, J.P.; Lehtinen, K.E.J.; Yli-Juuti, T. Optimization of process models for determining volatility distribution and viscosity of organic aerosols from isothermal particle evaporation data. *Atmos. Chem. Phys.* **2019**, *19*, 9333–9350. [CrossRef]

29. Yli-Juuti, T.; Pajunoja, A.; Tikkanen, O.-P.; Buchholz, A.; Faiola, C.; Väisänen, O.; Hao, L.; Kari, E.; Peräkylä, O.; Garmash, O.; et al. Factors controlling the evaporation of secondary organic aerosol from α-pinene ozonolysis. *Geophys. Res. Lett.* **2017**, *44*, 2562–2570. [CrossRef]

30. Jiang, J.; Aksoyoglu, S.; El-Haddad, I.; Ciarelli, G.; Denier van der Gon, H.A.C.; Canonaco, F.; Gilardoni, S.; Paglione, M.; Minguillón, M.C.; Favez, O.; et al. Sources of Organic Aerosols in Europe: A Modeling Study Using CAMx with Modified Volatility Basis Set Scheme. *Atmos. Chem. Phys.* **2019**, *19*, 15247–15270. [CrossRef]

31. Chen, X.; Yang, W.; Wang, Z.; Li, J.; Hu, M.; An, J.; Wu, Q.; Wang, Z.; Chen, H.; Wei, Y.; et al. Improving New Particle Formation Simulation by Coupling a Volatility-Basis Set (VBS) Organic Aerosol Module in NAQPMS+APM. *Atmos. Environ.* **2019**, *204*, 1–11. [CrossRef]

32. Zhao, Y.; Nguyen, N.T.; Presto, A.A.; Hennigan, C.J.; May, A.A.; Robinson, A.L. Intermediate Volatility Organic Compound Emissions from On-Road Gasoline Vehicles and Small Off-Road Gasoline Engines. *Environ. Sci. Technol.* **2016**, *50*, 4554–4563. [CrossRef] [PubMed]

33. Alam, M.S.; Zeraati-Rezaei, S.; Xu, H.; Harrison, R.M. Characterization of Gas and Particulate Phase Organic Emissions (C9–C37) from a Diesel Engine and the Effect of Abatement Devices. *Environ. Sci. Technol.* **2019**, *53*, 11345–11352. [CrossRef] [PubMed]

34. Lu, Q.; Zhao, Y.; Robinson, A.L. Comprehensive Organic Emission Profiles for Gasoline, Diesel, and Gas-Turbine Engines Including Intermediate and Semi-Volatile Organic Compound Emissions. *Atmos. Chem. Phys.* **2018**, *18*, 17637–17654. [CrossRef]

35. Anderson, M.; Salo, K.; Hallquist, Å.M.; Fridell, E. Characterization of Particles from a Marine Engine Operating at Low Loads. *Atmos. Environ.* **2015**, *101*, 65–71. [CrossRef]

36. Alanen, J.; Isotalo, M.; Kuittinen, N.; Simonen, P.; Martikainen, S.; Kuuluvainen, H.; Honkanen, M.; Lehtoranta, K.; Nyyssönen, S.; Vesala, H.; et al. Physical Characteristics of Particle Emissions from a Medium Speed Ship Engine Fueled with Natural Gas and Low-Sulfur Liquid Fuels. *Environ. Sci. Technol.* **2020**, *54*, 5376–5384. [CrossRef]

37. Alanen, J.; Simonen, P.; Saarikoski, S.; Timonen, H.; Kangasniemi, O.; Saukko, E.; Hillamo, R.; Lehtoranta, K.; Murtonen, T.; Vesala, H.; et al. Comparison of Primary and Secondary Particle Formation from Natural Gas Engine Exhaust and of Their Volatility Characteristics. *Atmos. Chem. Phys.* **2017**, *17*, 8739–8755. [CrossRef]

38. Onasch, T.B.; Trimborn, A.; Fortner, E.C.; Jayne, J.T.; Kok, G.L.; Williams, L.R.; Davidovits, P.; Worsnop, D.R. Soot Particle Aerosol Mass Spectrometer: Development, Validation, and Initial Application. *Aerosol Sci. Technol.* **2012**, *46*, 804–817. [CrossRef]

39. Petzold, A.; Hasselbach, J.; Lauer, P.; Baumann, R.; Franke, K.; Gurk, C.; Schlager, H.; Weingartner, E. Experimental Studies on Particle Emissions from Cruising Ship, Their Characteristic Properties, Transformation and Atmospheric Lifetime in the Marine Boundary Layer. *Atmos. Chem. Phys.* **2008**, *8*, 2387–2403. [CrossRef]

40. Timonen, H.; Teinilä, K.; Barreira, L.; Saarikoski, S.; Simonen, P.; Dal Maso, M.; Keskinen, J.; Kalliokoski, J.; Moldonova, J.; Salberg, H.; et al. *SCIPPER Project Deliverable D3.3 Ship on-Board Emissions Characterisation*; EU: Maastricht, The Netherlands, 2022.

41. Kautzman, K.E.; Surratt, J.D.; Chan, M.N.; Chan, A.W.H.; Hersey, S.P.; Chhabra, P.S.; Dalleska, N.F.; Wennberg, P.O.; Flagan, R.C.; Seinfeld, J.H. Chemical Composition of Gas- and Aerosol-Phase Products from the Photooxidation of Naphthalene. *J. Phys. Chem. A* **2010**, *114*, 913–934. [CrossRef]

42. Jalkanen, J.-P.; Brink, A.; Kalli, J.; Pettersson, H.; Kukkonen, J.; Stipa, T. A Modelling System for the Exhaust Emissions of Marine Traffic and Its Application in the Baltic Sea Area. *Atmos. Chem. Phys.* **2009**, *9*, 9209–9223. [CrossRef]

43. Jalkanen, J.-P.; Johansson, L.; Kukkonen, J.; Brink, A.; Kalli, J.; Stipa, T. Extension of an Assessment Model of Ship Traffic Exhaust Emissions for Particulate Matter and Carbon Monoxide. *Atmos. Chem. Phys.* **2012**, *12*, 2641–2659. [CrossRef]

44. Agrawal, H.; Welch, W.A.; Miller, J.W.; Cocker, D.R. Emission Measurements from a Crude Oil Tanker at Sea. *Environ. Sci. Technol.* **2008**, *42*, 7098–7103. [CrossRef] [PubMed]

45. Sippula, O.; Stengel, B.; Sklorz, M.; Streibel, T.; Rabe, R.; Orasche, J.; Lintelmann, J.; Michalke, B.; Abbaszade, G.; Radischat, C.; et al. Particle Emissions from a Marine Engine: Chemical Composition and Aromatic Emission Profiles under Various Operating Conditions. *Environ. Sci. Technol.* **2014**, *48*, 11721–11729. [CrossRef] [PubMed]

46. Reichle, L.J.; Cook, R.; Yanca, C.A.; Sonntag, D.B. Development of Organic Gas Exhaust Speciation Profiles for Nonroad Spark-Ignition and Compression-Ignition Engines and Equipment. *J. Air Waste Manag. Assoc.* **2015**, *65*, 1185–1193. [CrossRef]

47. Grigoriadis, A.; Mamarikas, S.; Ntziachristos, L.;Majamäki, E.; Jalkanen, J.-P. *SCIPPER Project Deliverable D4.1 New Set of Emission Factors and Activity Information*; EU: Maastricht, The Netherlands, 2021.